TEMPORAL LINKAGES BETWEEN NEARSHORE BATHYMETRY, SHORE ICE MORPHOLOGY, AND GEOMORPHIC CHANGE ALONG A COLD-CLIMATE COASTLINE

By

Brittany M Hartley

A THESIS

Submitted to
Michigan State University
in partial fulfillment of the requirements
for the degree of

Geography—Master of Science

2022

ABSTRACT

TEMPORAL LINKAGES BETWEEN NEARSHORE BATHYMETRY, SHORE ICE MORPHOLOGY, AND GEOMORPHIC CHANGE ALONG A COLD-CLIMATE COASTLINE

By

Brittany M Hartley

The nearshore ice complex (NIC) though previously studied, has given researchers muddled conclusions when studies are compared, as the documented morphological response to ice presence has been varied. This blurriness of understanding promoted the opportunity for research, and with the availability of new and improved technology, an opportunity for high accuracy analysis also arises. This study showed that ice ridge location corresponded to the bar and trough system in lakebed morphology, rather than just a nearshore bar or trough. Along with that, the ice presence lowered the overall elevation of the lakebed profile, and this promoted erosion throughout the remainder of the study period. During the entirety of the research study period, the most change that was documented was found between August and November 2020 due to a large, recoded storm event that moved through the study location

ACKNOWLEDGEMENTS

I would like to acknowledge and thank Michigan State University, the Department of Geography, the College of Social Science, and the National Science Foundation for the opportunity to advance my academic understanding and for the support throughout my program. I would also like to thank Dr. Ethan Theuerkauf, my advisor, who supported me through every high and low during this experience, and my committee member Dr. Julie Winkler and Dr. Nathan Moore.

TABLE OF CONTENTS

LIST OF TABLES v

LIST OF FIGURES vi

KEY TO ABBREVIATIONS vii

Introduction 1
Ice morphology and nearshore bathymetry 3
Morphological changes 6

Methods 9
Study Area 9
Hydrodynamics 11
Ice 12
Field Surveys and Analysis 12

Results 18
Hydrodynamics 18
Shore Ice Extent 21
Ice morphology and nearshore bathymetry 23
Morphological changes 24

Discussion 29
Ice morphology and nearshore bathymetry 29
Morphological changes 31
Conceptual Model 34

Conclusions 36

REFERENCES 37

LIST OF TABLES

Table 1: A summary table of the peak significant wave height measured in meters during the time series between surveys.....20

Table 2: A summary table of the average significant wave height measured in meters during each time series 20

Table 3: A summary table of the average water level measured in meters during each time series between surveys 20

Table 4: A summary table of case study morphological results. Description of time series given with rank of influence throughout the study period.....24

LIST OF FIGURES

Figure 1: Site area map of Chocolay Beach below the roadside park on Michigan state highway M28 in Marquette, MI. Located along the southern Lake Superior shoreline.....10

Figure 2: A data collection flow chart for field surveys and subsequent data processing for creating a topobathymetric map.....17

Figure 3: The significant wave height for the entire study period August 2020-September 2021 was graphed using Grapher software. Vertical red lines were plotted as survey dates to show wave activity between each survey. A significant wave event in November 2020 was noted with a black arrow.....19

Figure 4: Digitized ice extent lines over the December 16, 2021 topobathymetric map.....22

Figure 5: Profiles of ice morphology and December, March, and September bathymetry on the nearshore derived from two transects A-A' and B-B' run perpendicular to the shoreface. Red dashed lines overlay the profiles noting the relationship between the ice morphology and the December bathymetry profile 23

Figure 6: Topobathymetric maps from all surveys conducted. August, November, and December of 2020 and, March, and September of 2021 surveys are displayed with elevation range of 194-178 meters.....25

Figure 7: DEMs of Difference (DOD) between each of the surveys. August 8, 2020- November 04, 2020, November 04, 2020- December 16, 2020, December 16, 2020- March 30, 2021, March 30, 2021- September 20, 2021 are the time series combinations.....26

Figure 8: Elevation profiles from the March 30, 2021 and September 20, 2021 surveys accompanied by corresponding water levels to represent the shoreline position on those dates.……...……...……..28

Figure 9: December 16, 2021 DEM of difference. A) Bar of accretion, B) Area of erosion, example z = -1.16 meters. December 16, 2021 DEM of difference accompanied by digitized lines of lakeward ice extent from Planet satellite imagery 31

Figure 10: Conceptual model of case study results. Showing the profile change encompasses the trifecta of morphological events; Fall Storms, Ice Generation, and Ice Recession, that are all based on the same fundamental driving force; hydrodynamic activity, specifically wave action.……...……..…35

KEY TO ABBREVIATIONS

NIC	Nearshore Ice Complex
DEM	Digital Elevation Model
DOD	DEM of Difference
GLERL	Great Lakes Environmental Research Laboratory
NAVD88	North American Vertical Datum of 1988

Introduction

Cold climate coastlines make up around 30% of the global coastline (Lantuit et al.,2011) and are important from both socio-economic and environmental perspectives. These cold climate regions have a documented economic output per capita that is up to 12 times larger than mid-latitudes and more temperate regions (Nordhaus, 2006). From an environmental perspective, these cold-climate coastal areas contain permafrost which is a major carbon sink and plays an important role in nutrient cycling and biogeochemical processes (Douglas et al., 2014). Despite these benefits cold-climate coastlines are highly vulnerable to rising sea levels, atmospheric warming, and associated coastal hazards such as erosion (US EPA, 2016). Some aspects of climate change impacts on cold coasts, such as permafrost melting, have received substantial research attention, particularly in the United States (Philipp et al., 2021). Others such as coastal geomorphic changes and processes associated with shore ice are less understood. The paucity of research on shore ice-related erosion and sediment transport has led to shore ice not being incorporated in coastal evolution models nor in coastal planning and management.

This study contributes to addressing this knowledge gap by first describing the relationship between nearshore bathymetry and shore ice morphology using cutting-edge remote sensing technology and then documenting the mechanisms of sediment transport and associated geomorphic changes associated with winter shore ice. These changes are then placed into a temporal context with other coastal processes that facilitate change, such as storms and littoral transport, to better understand the role ice plays in annual coastal change.

Previous studies have indicated opposing impacts of shore ice on coastal geomorphic change and sediment transport (BaMasoud and Byrne, 2012; Theuerkauf et al. 2021; O'Hara and Ayers, 1972; O'Hara, 1972; Barnes et al., 1994; Barnoff-Nielsen, 1988) some studies indicate

the presence of ice protects the beach while others indicate that ice induces and enhances coastal erosion. The prevailing assumption of shore ice influence is that the presence of shore ice affords a protective benefit to the beach and nearshore during the winter. Specifically, it is thought that ice buffers the shoreface from wave energy impacts (Forbes and Taylor, 1994), and previous studies have indicated that when ice is absent there is an increase in coastal erosion (BaMasoud and Byrne, 2012; Theuerkauf et al. 2021; O'Hara and Ayers, 1972; Dionne and Laverdiere, 1972; Marsh et al., 1976; Davis, 1973; Davis et al., 1976; Evenson and Cohn, 1979). Other studies suggest that when present ice protects the beach from winter storm waves, but when ice deteriorates it can erode the nearshore and transport sediments within and potentially out of the nearshore environment (O'Hara, 1972; Barnes et al., 1994; Barnoff-Nielsen, 1988). Previous studies have observed scour of the lakebed at the lakeward edge of the shore ice (Barnes, 1990, 1993, 1994; Bajorunas and Duane, 1967) and due to wave breaking and energy deflection down towards the bed (Barnes, 1990, 1993, 1994). This can occur when the ice is stable as well as when the ice is deteriorating. Some studies outright indicate that ice breakup and subsequent transport of brash and slush can erode and transport large volumes of sediment offshore (Kempema and Holman, 1994). These studies allude to the dynamic relationship between nearshore bathymetry, shore ice, and geomorphic change and sediment transport; however, a mechanistic understanding of this relationship remains elusive. This presents a challenge for being able to accurately model the role of shore ice in coastal evolution, which is ultimately needed for predicting future coastal change in these regions and conducting proactive coastal management.

Ice morphology and nearshore bathymetry

The nearshore ice complex (NIC) is most abundant on sandy shorelines exposed to high wave action (Barnes et al., 1992). A well-developed NIC requires the right combination of air and water temperature, winds and waves, and open water with a supply of ice fragments (Bryan and Marcus 1972; Marsh et al 1973). The degree of NIC growth is spatially variable and areas with shoreline protection, such as harbor jetties, tend to have an underdeveloped NIC or lack it entirely (Barnes et al., 1994). Formation of the NIC proceeds from the beach out into the lake and starts with the formation of an icefoot on a frozen beach (Barnes et al., 1994). Lakeward growth of the NIC follows genesis of the icefoot (Barnes et al., 1994). Grounded ice ridges form at the lakeward edge of the complex, where high-energy waves makes contact with the shore ice, and have been documented in previous studies to be spatially related to nearshore bars (Barnes et al., 1994). Following this, wave action continues to build out the complex with additional ridges with intervening ice lagoons that appear to represent quiescent periods (Barnes et al., 1994). Lakeward of the ice ridges is a zone of brash and slush ice (Barnes et al., 1994), which is both a key ingredient in the formation of ice ridges but can also be formed from the deterioration of the NIC. The brash and slush ice can be formed into ice ridges by wave attack against the evolving NIC (e.g. Barnes et al., 1994). The NIC is highly dynamic during the winter and can change rapidly in response to storms and temperature variations (Marsh et al., 1973).

Prior research has indicated that ice ridges are primarily associated with underlying nearshore bars on lakebed bathymetry (Siebel et al., 1976), but also note that ice ridges outnumber offshore bars in some cases (Barnes et al., 1994). It is logical that ice ridges are spatially associated with nearshore bars given that wave breaking, and associated spray and splash are considered the primary processes forming ridges (Bryan and March 1972). While

wave attack and associated thrust processes can result in ice and sediment piling up into ridges, it can also lead to scour in front of the ice as wave energy is diverted down to the bed after it makes contact with the ice front (Barnes et al., 1990). Previous work has likened this to the process of nearshore scour that results from wave interaction with seawalls (Barnes et al 1990, Barnes et al., 1994) This has been documented in both lacustrine environments as well as in ocean environments along the seaward landfast ice edge (SLIE) (Mahoney et al., 2005). This nearshore scour has been previously documented to be very local (i.e., immediately outboard of the ice edge) and ephemeral, as it has been suggested that the processes of ice decay and associated sediment transport should fill in these scour zones (Bajorunas and Duane 1967; Barnes et al., 1990).

Shore ice-associated processes are just one category of coastal processes at work during an annual period. Other coastal geomorphic processes, including littoral drift and storm-induced erosion and accretion, evolve the nearshore morphology and likely alter or enhance the impacts of shore ice. Storm events can induce cross-shore sediment transport, where sand is moved onshore and offshore via bar migration and/or overwash. Sediment can also be transported alongshore via littoral drift, which occurs during the recorded storm event as well as typical wave conditions. The natural cross-shore and alongshore sediment transport patterns can be augmented by coastal infrastructure as well as shore ice. Shore normal coastal infrastructure, such as jetties and groins, impede littoral drift and lead to excess sand deposition on the updrift side and sand starvation on the downdrift side. Shore perpendicular oriented shore protection infrastructure, such as seawalls and revetments, leads to scouring and offshore sediment transport as wave energy is transmitted down to the bed. Shore ice augments, changes, patterns of nearshore sediment transport, primarily via a lakeward shift of the zone of sediment transport

when ice is present. This results in a reduction in sediment transport in the area protected by ice but may enhance sediment transport lakeward of the ice in a similar fashion to shore parallel structures. During ice breakup, complex changes in patterns of nearshore sediment transport occur in poorly understood ways. These sediment transport processes lead to patterns of erosion and accretion that alter the nearshore morphology. Accretion in the nearshore may lead to lakeward movement of the shoreline and cross-shore bar migration and vertical growth. Erosion can also occur in response to sediment transport, which changes the distribution of sediment in the nearshore. It is important to note that erosion and deposition can occur even during non-storm conditions if the nearshore profile is out of equilibrium or if shore ice is present. With respect to shore ice, erosion has been documented in association with the breakup process as well as in front of the NIC. Deposition has been observed to occur in association when the NIC melts in place or when waves break apart the NIC and redistribute the entrained material.

Water level can also modulate patterns of sediment transport in the nearshore zone. The role of water level in facilitating coastal change is well-documented (e.g., Meadows et al., 1997; Theuerkauf et al., 2019, 2021, etc.). High water levels facilitate wave erosion of more landward portions of the coastal system, such as the backshore, dunes, and bluffs. In the Great Lakes environment, there has been a substantial amount of coastal habitat loss due to fluctuating lake levels (Theuerkauf and Braun 2021), and it was noted that higher amounts of recorded property damage recorded to correspond to times of increased wave energy (Meadows et al., 1997). In a marine environment sea level anomalies and increases in water level, combined with rapid sea-level rise and storm frequency variability, correspond to high erosive impacts (Theuerkauf et al., 2014).

The NIC has been documented to contain a sediment load that equals the sediment load eroded from coastal bluffs and a load of sand trapped within shore ice that is rafted offshore, potentially past the depth of closure (Barnes et al., 1994). Despite that study, and despite the acknowledgment of the importance of sea-ice sediment transport to the overall sediment budget, the processes involved are still not fully understood (Kempema, Reimnitz, and Barnes, 1989). Understanding the primary geomorphic processes that occur in association with NIC development, specifically ice morphology development, is fundamental and essential to current Great Lakes research. Primary processes that affect NIC development are still being researched and connections are yet to be made between ice stage development and the consequential geomorphic response of the shoreface and underlying bathymetry.

Morphological changes

There is a prevailing course of thought that the nearshore ice complex (NIC) guards the shoreline, creating a protective barrier against harsh winter hydrodynamic processes (Kempema and Holman, 1994; Evenson and Cohn, 1979; Marsh et al., 1973; BaMasound and Byrne, 2012;Forbes and Taylor, 1994; Barnes et al., 1994; McCann and Taylor, 1975; Bryan and Marcus, 1973; O'Hara and Ayers, 1972; Bajorunas and Duane, 1967; Miner and Powell, 1991). Other studies agree that while the ice complex is present it acts as a protective barrier against hydrodynamic processes like wave action but go on to acknowledge that when ice deterioration initiates, it erosively moves sediment around or potentially out of the nearshore environment (O'Hara and Ayers, 1972; Barnes et al., 1993, 1994; Bajorunas and Duane, 1967; Miner and Powell, 1991; Barnoff-Nielsen, 1988; Hayden et al., 1992). The significance of this presented work is shown through differences in opinion in literature on the impacts of shore ice presence,

as this study is presenting the opportunity to participate in the discussion of morphological change associated with shore ice.

The NIC can serve to protect the shoreline during the winter months (O'Hara and Ayers 1972; Davis, 1973; Evenson and Cohn 1979). This is done through the NIC generating ice ridges where the beach is protected along the shoreline and erosion is little to none (Forbes and Taylor, 1994). It has been documented that the icefoot works to provide the last effort protection barrier from high energy waves that cause high erosion. In comparison to ice-free shoreline portions, the ice foot provides significant protection based on sediment transport (Marsh et at. 1973). However, it is possible that in lieu of erosion being negated it is being diverted offshore, or alternatively through other passage zones differing from the broad approach toward the shoreline.

Most other studies argue that shore ice presence and processes can lead to enhanced erosion (Barnes et al., 1994, BaMasoud and Byrne, 2012, Hequette, Desrosiers, and Barnes, 2015, Miner and Powell, 1991). These studies are based on onshore ice being anchored to the shoreface, and the erosion process begins at the initiation of the ice break-up process. This referenced erosion is founded on the assumption of there being sand entrained within the shore ice. This entrainment occurs during NIC development and ice-push and thrust processes. The sediment entrained ice breaking up, especially if the break up process occurs multiple times, allows for the opportunity for that material to be transported offshore through wind-driven transport and melting processes. Notably, in previous literature, it was proposed that coastal ice transports sediments offshore, but one study showed that under certain circumstances after sediment-laden ice was transported offshore, it was transported to the opposite side of the lake (Reimnitz et al. 1991).

Climatic changes altering temperatures and ice concentrations (Wang et al. 2012, 2017; Baumann and Doherty 2013) are leaving more open-water ice seasons exposing the shorelines to wave energy and winter storms (BaMasound and Bryne, 2012). Atmospheric conditions dictate that shallow water lakes freeze faster and develop ice earlier in the ice season as opposed to deep water lakes. This lag in ice onset was documented along with ice cover showing a long-term declining trend of 66% of ice cover lost over the Great Lakes over a 45-year time span (Wang, 2017).

This study investigates the relationship between nearshore bathymetry and ice morphology through quantitative analysis during a year-long study period and the consequent impact relative to the rest of the year and physical processes. Through measuring annual geomorphic change, the role of shore ice in the total annual behavior can be extracted, illuminating its' contribution to the changes in nearshore evolution. The quantitative aspect of this investigation is a key contribution to current known research as it provides the opportunity to provide more detailed account of geomorphic change. This work highlights nuances in the relationship between ice morphology, specifically ice ridges, and the nearshore bathymetry, acknowledges the persistence and magnitude of morphological change and the potential long-term interpretation of relevant coastal processes, and discusses the interplay between the temporal linkages between annual coastal processes.

Methods

Study Area

This study focuses on Chocolay Beach, which is a sandy beach site located along the southern Lake Superior shoreline (Figure 1). It is situated at the base of a sandy bluff and is accessed via the Lake Superior Roadside Park on M28 in Chocolay Charter Township, Michigan. The study location area spans 0.18 kilometers in width by 0.26 km in length. Historical aerial imagery viewed in Google Earth Pro reveals that over the past three decades this beach has shown a cyclical pattern of sandy bars migrating alongshore from west to east via periodic welding and detachment from the shoreline. This site was an ideal candidate for this shore ice study as Lake Superior reliably has shore ice present given the prevalence of winter ice cover (long-term average of 64% ice cover; GLERL, 2021). Additionally, this is an open-coast site that is exposed to large wave events from the north as well as fluctuating lake levels on seasonal, annual, and decadal timescales. These physical conditions provide an opportunity to study the relationship between winter shore ice and coastal geomorphic changes along wave dominated cold-climate coastlines

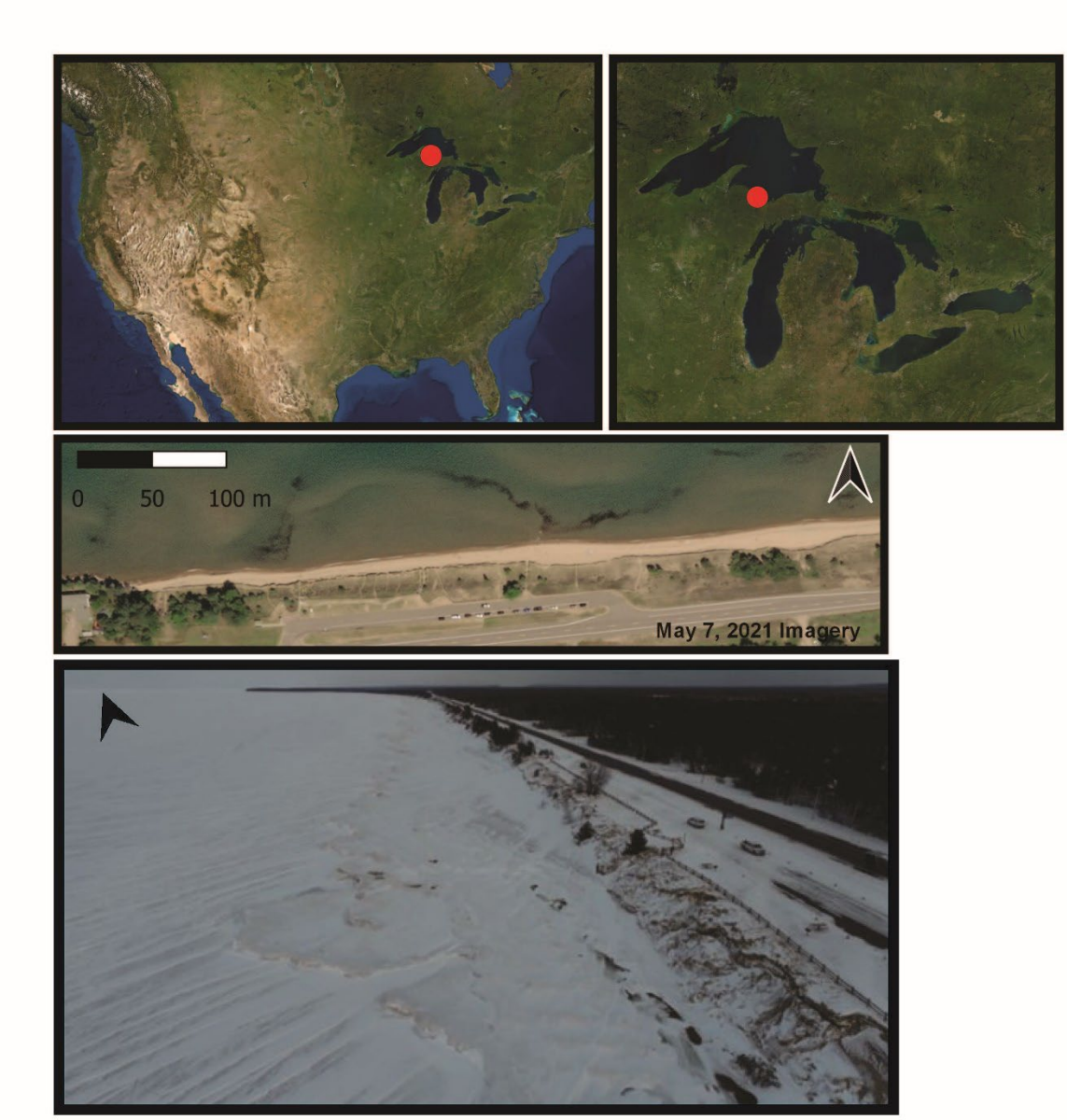

Figure 1: Site area map of Chocolay Beach below the roadside park on Michigan state highway M28 in Marquette, MI. Located along the southern Lake Superior shoreline.

Hydrodynamics

Wave and water level data were gathered to document the hydrodynamic processes at the study site during the monitoring period from August 8, 2020 through September 20, 2021. Hourly water level data were gathered from NOAA for the Marquette Coast Guard Station (Station ID: 9099018; NOAA Tides and Currents). This station is approximately 13.04 kilometers NW of the study site. The water level elevation data were converted from IGLD85 to NAVD88 by subtracting 0.0173 meters. This was completed because all topographic and bathymetric elevation data generated in this study use NAVD88 as the vertical datum. Hourly significant wave height data, significant wave height being defined as the aberage top 1/3 of wave heights present, were acquired from the Great Lakes Coastal Forecasting System (GLCFS) from the NOAA Great Lakes Environmental Research Laboratory (GLERL). For part of the study period (August through December 2020) the GLCFS used the Princeton Ocean Model (Blumberg and Mellor, 1987) and the GLERL-Donelan wave model (Schwab et al., 1984) to predict waves. Starting January 1, 2021 the GLCFS transitioned to the Finite Volume Community Ocean Model (FVCOM; GLERL, 2021).

The wave and water level data were divided into time bins defined by being the time in between the geomorphic change field surveys and then analyzed to derive descriptive statistics for each of these bins. The significant wave height data were input into a RStudio script summary code to produce statistics including the average, maximum, and minimum wave height for each of the time bins. These statistics were exported from R and compiled into a table in Microsoft Excel. Corrected water level data were used to denote the position of the shoreline on the topobathymetric maps as well as the profiles extracted. This intersection denotes the division between the subaerial (beach and bluff) and subaqueous (nearshore) zones.

Ice

Satellite imagery products were collected from Planet using Planet Explorer in order to map the lakeward extent of shore ice during the winter ice season at the study site. Planet uses 200 Dove CubeSat satellites daily to collect imagery of the physical Earth. This imagery was sourced through 4-band PlanetScope Scene by satellite ID 0f15 at 3-meter pixel resolution and ground sample distance of approximately 4 meters. Requested imagery of approximately 4.2 kilometers in length and 0.9 km in width were downloaded to ensure full coverage of the study site in order to track the nearshore ice complex progression over the 2021 winter ice season. Planet satellite imagery were downloaded from mid-January 2021 through the end of March 2021. Only 13 of the 19 downloaded images were cloud-free and usable for mapping shore ice extent. From these 13 images where the site and associated ice were clearly visible, the lakeward extent of the nearshore ice complex was digitized in ArcMap 10.3. Shapefiles were created from these digitized ice lines to evaluate spatial relationships between ice extent and geomorphic change.

Field Surveys and Analysis

Field Surveys were conducted in August 8, 2020, November 4, 2020, December 16, 2020, and February 18, 2021, March 30, 2021, and September 20, 2021. During all field excursions except February 2021, topography data were collected (Figure 2) with a drone, bathymetry were collected with a remote-controlled catamaran, and swash and inner surf zone morphology were mapped with RTK-GPS wading surveys (Figure 2). Only drone topography data were collected in the February 2021 field excursion to map the ice morphology when the NIC was fully developed.

Drone flights with a DJI Phantom 4 Pro V2.0 small unoccupied aerial system (sUAS) were conducted over Chocolay beach to collect high- resolution ground imagery with less than 2-centimeter accuracy (Figure 2). This imagery was utilized to derive a digital elevation model (DEM) of the subaerial site topography (shoreline landward to the sandy bluff). A 1-inch, 20-megapixel RGB sensor on a gimbal-mounted camera was mounted on the drone. Preprogrammed flight plans were created and executed in DJI Ground Station Pro. Flight parameters include 80% front and side overlap, only nadir (downward-facing) imagery, and a flight altitude of 53.5m with a resolution of 1.5 centimeters per pixel. Immediately prior to the flight, approximately a dozen 1 foot by 1 foot black and white targets were placed throughout the subaerial portion of the site as ground control points (GCPs) to spatially reference the drone imagery. These GCPs were surveyed with a Trimble R10-2 GNSS system, which provided XYZ positioning of the GCPs with around 3 cm horizontal and vertical error.

Drone-collected imagery was processed using structure-from-motion photogrammetry implemented in Agisoft Metashape Professional (Figure 2). In the software the images were checked for quality and aligned. Then, GCP survey data were imported, and the black and white targets were identified in the imagery to spatially reference the images. From here, the software implements structure-from-motion photogrammetric algorithms to build a dense point cloud. This dense point cloud was then utilized to produce DEMs and orthomosaic images. The DEMs were exported as ASCII grid files with 0.5 m grid spacing and orthomosaic images are exported as TIFF files with pixel resolution of 0.05 meters, with this being the final resolution product of the DEM. The DEM was imported into Surfer and a contour map was created with 0.2m contour intervals. The XYZ data from this contour map was exported as an ASCII file from Surfer in order to be combined with the bathymetry data to create a seamless topobathymetric map for

each survey (Figure 2). sUAS imagery is useful for mapping subaerial topography, but cannot penetrate water, therefore, a remotely operated surface vehicle and wading surveys were utilized to map bathymetry.

A Seafloor Systems HyDrone remotely controlled catamaran equipped with a Seafloor Systems SonarMite single beam echosounder and a Trimble R10-2 GNSS system was deployed to collect bathymetric data continuously throughout deployment at the study site (Figure 2). This instrument was only deployed during calm wave conditions to minimize vessel roll that would lead to noisy and erroneous data. Bathymetry data were collected primarily along shore-normal transects, however some additional data were gathered along parallel lines to reduce gridding artifacts. The sonar and the GNSS system work together to gather horizontal and vertical position data every time a depth sounding is made (approximately every 2 seconds). The GNSS system is recording the XYZ position of the transducer, the sonar is acquiring the depth, and when combined lakebed elevation is mapped. Lakebed elevation data were exported into Microsoft Excel, corrected for the GNSS antenna height and cleaned to remove spurious data points. Any points with a depth lower than 0.5 meters were deleted from the dataset because this is below the resolution of the instrument and thus is likely to result in noise artifacts. Given this depth limitation, there is a spatial gap between the coverage from the sonar survey and the drone topography survey which was filled with a RTK-GPS wading survey.

The Trimble R10-2 GNSS system was utilized to conduct wading surveys (Figure 2). The GNSS antenna is mounted on a 2.0m pole and surveys were conducted along shore normal transects spaced approximately ~15 meters apart. Wading surveys began at the shoreline and proceeded lakeward to wading depth (approximately 1m water depth). These data were exported

from the Trimble Survey Controller and brought into Golden Software's Surfer and Microsoft Excel for combination with drone topography and sonar bathymetry data as well as cleaning.

The final step in cleaning the morphology data was to remove overlap between the bathymetry and wading survey data. Both sets of data points were visualized in Surfer and overlapping points were identified. Where there was overlap, the sonar data point was removed as the wading survey is considered more accurate given that the lakebed elevation was physically surveyed as opposed to remotely sensed with the sonar. This cleaned dataset was then combined with the XYZ data from the drone DEM into one dataset. These data were then gridded in Surfer using the Natural Neighbor algorithm to create a 5-m-spaced topobathymetric grid, which was then used to generate a seamless topobathymetric contour map (Figure 2).

The topobathymetric maps from each of the surveys were of varying alongshore and across-shore dimensions, thus, to make meaningful comparisons between each survey they had to be normalized to a standard size. A box of 200m x 400m dimensions was created to normalize the alongshore dimension and then the Blanking function in Surfer was implemented to remove data outside of this box. Similarly, a fixed position landward of the bluff crest was used as the landward boundary of each topobathymetric map and data landward of this line was blanked out. These blanked topobathymetric grids were then subtracted from each other using Surfer's Grid Math function to derive DEMS of Difference (DODs), which quantify elevation change and allow visualization of spatial patterns of erosion and accretion. With this function, the more recent topobathymetric grid was subtracted from the older grid to generate a grid of elevation change between the two surveys. This was conducted for each consecutive survey (e.g., November 2020 to August 2020) and then the output grid was used in Surfer to construct a contour map of elevation change, referred to here as subtraction maps. In these subtraction maps,

red colors denote erosion, white represents little to no change, and blue represents accretion. Volume change was estimated using the Volume function in Surfer in order to quantify the change between each survey. Net volume (erosion + accretion) and positive and negative planar area were recorded for each of the subtraction maps. Even though the site dimensions were constrained with the blanking boxes, there were still some areal differences between surveys due to mapping coverage differences and data gaps, thus the net volume change computed from the DODs was normalized by the total (positive + negative) planar area. Furthermore, since the time elapsed between each survey period was different, this normalized volume was also divided by the amount of time elapsed (in years) between surveys (Equation 1). This generated a standardized metric that can be compared across time periods in order to evaluate geomorphic changes from storms and shore ice.

$$\frac{\left(\frac{Net\ Volume}{(Positive\ Planar\ Area + Negative\ Planar\ Area)}\right)}{Time\ Elapsed}$$

Equation 1: Equation for calculating net volumetric change.

To evaluate the relationship between shore ice morphology and nearshore bathymetry, shore normal profiles were extracted from the December 2020 topobathymetric map as well as the February 2021 ice topography map. Two transects spaced approximately 40 m apart were created and elevation data were extracted across these transects for each survey using Surfer. These elevation data were then brought into Golden Software's Grapher program to plot the profile data and visualize the spatial relationships between ice morphology and nearshore bathymetry. Water level at the time of the surveys was also plotted to denote the shoreline position along the profile.

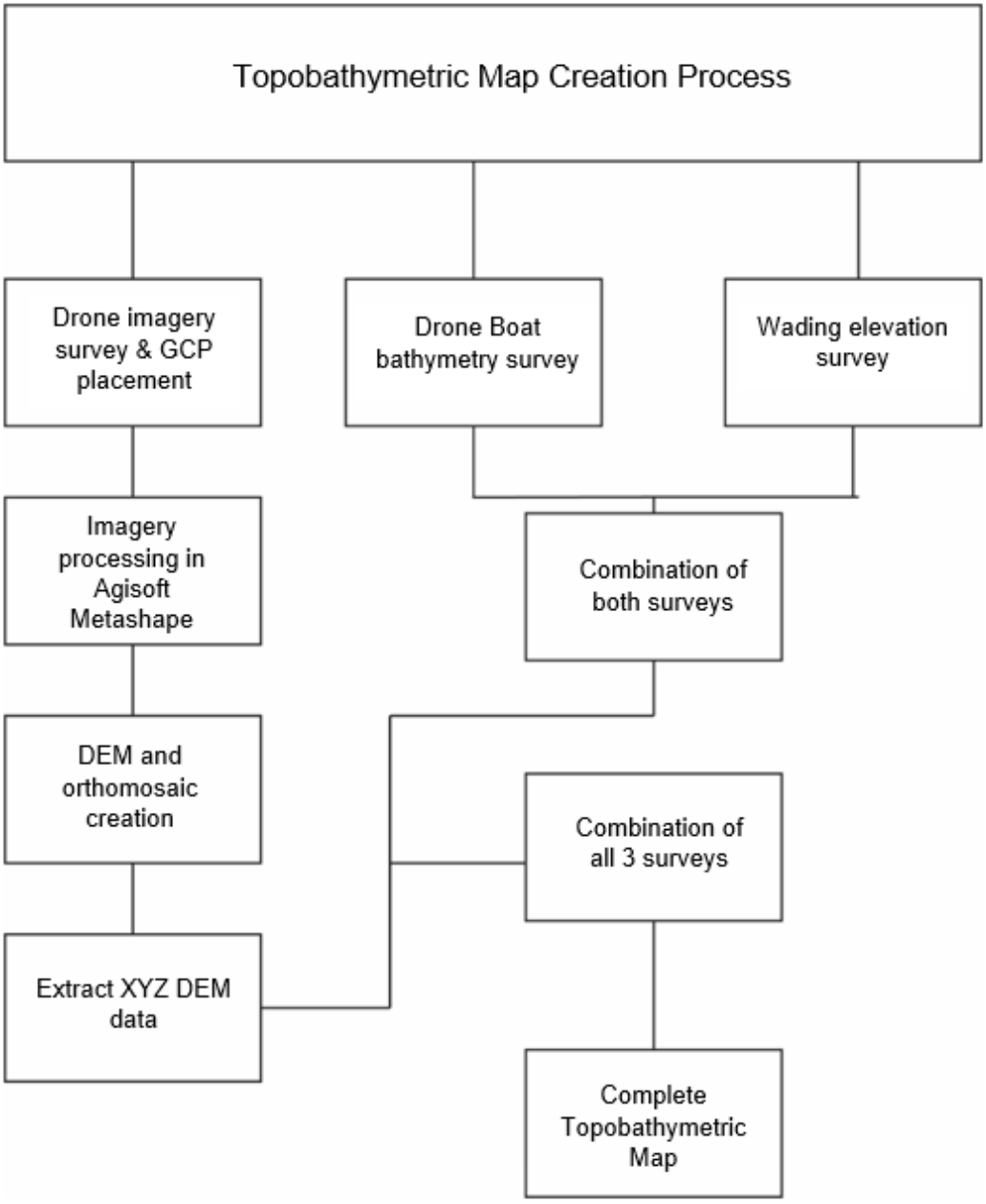

Figure 2: A data collection flow chart for field surveys and subsequent data processing for creating a topobathymetric map.

Results

Hydrodynamics

In the Great Lakes, significant wave heights greater than 2m are considered a storm event (Hubertz, 1992). From August 2020 to November 2020, the dominant hydrodynamic driver at the Chocolay site was a storm occurring on November 1, 2020 (Figure 3) with significant wave heights above the storm threshold. The peak significant wave height during this time was on November 1, 2020 with waves reaching a maximum of 4.069 meters (Table 1) and the average significant wave height was 0.54 meters (Table 2). During this time period, 2.4% of significant wave height observations were above the Great Lakes storm significant wave height (2m). The average water level during this time was 183.83 meters (NAVD88) (Table 3). While water level slightly fluctuates throughout the year, there was not so much change that it notably influences the surrounding processes. Water level is reported for documentation of in situ conditions timebin.

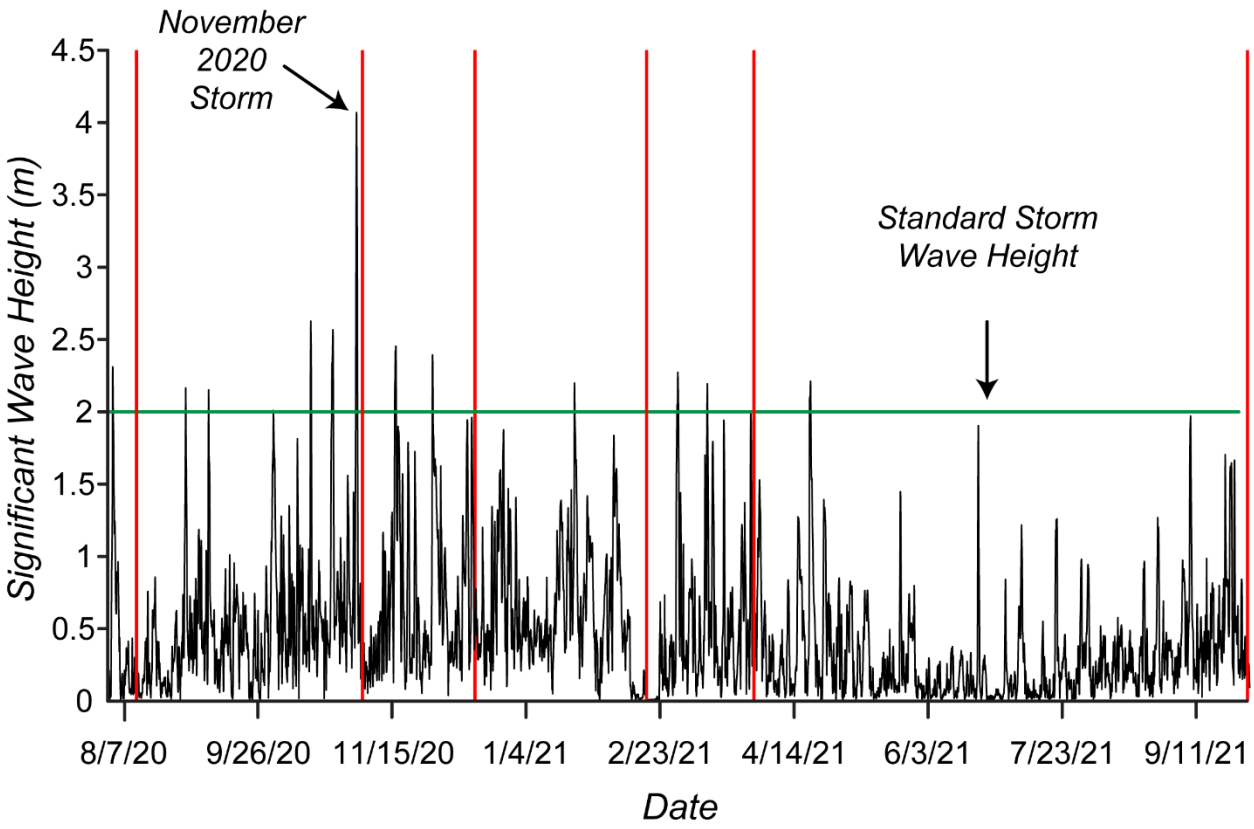

Figure 3: The significant wave height for the entire study period August 2020-September 2021 was graphed using Grapher software. Vertical red lines were plotted as survey dates to show wave activity between each survey. A significant wave event in November 2020 was noted with a black arrow.

The peak significant wave height during the period from November 2020 through December 2020 was 2.45 m, occurred only for a brief period, approximately one hour until the next observation collection. Most of this time period was characterized by calm wave conditions that are not likely to generate significant morphological changes (Table 1). The average significant wave height was 0.49 meters (Table 2). During this time series, 2.0% of significant wave height observations were above the Great Lakes storm significant wave height (2m). The average water level during this time was 183.76 meters (NAVD88) (Table 3).

Table 1: A summary table of the peak significant wave height measured in meters during the time series between surveys.

Time Series	Peak Significant Wave Height (m)
August 2020- November 2020	4.069
November 2020- December 2020	2.453
December 2020- February 2021	2.198
February 2021- March 2021	2.273
March 2021- September 2021	2.212

Table 2: A summary table of the average significant wave height in meters during each time series.

Time Series	Average Significant Wave Height (m)
August 2020- November 2020	0.54
November 2020- December 2020	0.49
December 2020- February 2021	0.61
February 2021- March 2021	0.49
March 2021- September 2021	0.31

Table 3: A summary table of the average water level measured in meters during each time series between surveys.

Time Series	Average Water Level (m)
August 2020- November 2020	183.83
November 2020- December 2020	183.76
December 2020- February 2021	183.59
February 2021- March 2021	183.47
March 2021- September 2021	183.56

From December 2020 to February 2021 which includes ice onset in January 2021, peak significant wave height was 2.198 meters (Table 1); however, only 0.26% of significant wave height observations were above the Great Lakes storm significant wave height indicating a generally calm period. Average significant wave height was 0.61 meters (Table 2) and the average water level during this time was 183.59 meters (NAD88) (Table 3). From February 2021 to March 2021, the period extending from the UAS ice morphology survey and ice-off, peak

significant wave height was 2.273 meters and 1.6% of significant wave height observations were above the Great Lakes storm significant wave height threshold. Average significant wave height is 0.49 meters (Table 2) and the average water level during this time was 183.5 meters (NAVD88) (Table 3).

In the time period between March 2021 and September 2021 peak significant wave height was 2.212 meters and only 0.25% of significant wave height observations were above the Great Lakes storm significant wave height threshold, indicating this was not a wavy period (Table 1). The average significant wave height was also low, 0.31 meters (Table 2), and the average water level during this time was 183.56 meters (NAVD88) (Table 3).

Shore Ice Extent

The development of the nearshore ice complex was based on the topobathymetric map derived from the December 16, 2020 survey. The nearshore ice complex had begun to form by January 30, 2021 (visible in satellite image on this day) and was present until March 20, 2021. After NIC initiation, it grew lakeward to a relatively stable position, represented by the February 21, 2021 ice extent line in red (Figure 4). From this location, the NIC stalled in growth until early March where it grew to a peak in development on March 7 (Figure 4). The NIC then receded from the March 7 ice extent to the March 13, where it lingered until approximately March 15, 2021 and completely deteriorated by March 20, 2021 (Figure 4).

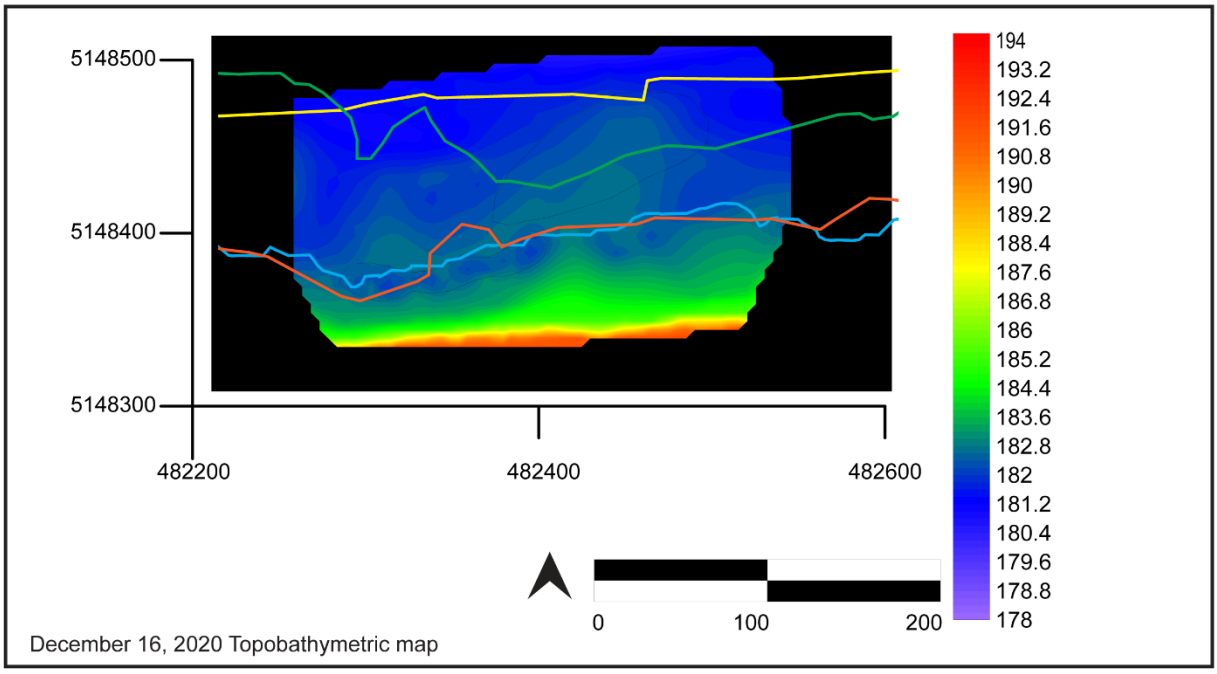

Figure 4: Digitized ice extent lines over the December 16, 2021 topobathymetric map.

This behavior shows that during the development and degradation of the NIC, there was a mappable average ice extent (Figure 4). The December topobathymetric map shows two occasions, February 21, 2021 and March 13, 2021, out of the 13 digitized ice extent lines to represent the average ice extent (Figure 4). Finally, the digitized ice extent lines for March 7 and 8 of 2021 illustrates the high variability of the lakeward edge of the ice complex. Between the two dates, up to 50 meters of ice degeneration occurred in a given day (Figure 4). This 24-hour span averaged significant wave height of 2.43 meters, higher than the standard 2 meter storm significant wave height of the Great Lakes region (Figure 3).

Ice morphology and nearshore bathymetry

During the December 2020 to February 2021 time series, the NIC formed and evolved. NIC morphology derived from the February 2021 UAS survey shows the first ridge developed over the initial depression in elevation located ~ 40-50 meters offshore (from the December 2020

profile; Figure 4). Profile 2 A-A' (Figure 5) shows the ice ridge to be at approximately 20 meters offshore of a shoreline at approximately 20 meters. This ice ridge location shows that there is approximately 2 meters between the ice ridge crest to the December profile trough (184 to 182 meters) (Figure 5, red dashed vertical lines). In Profile 3 B-B' (Figure 5, red dashed vertical lines) there is approximately 2 meters between the ice ridge crest to the December profile trough that is 30 meters offshore (184 to 182 meters).

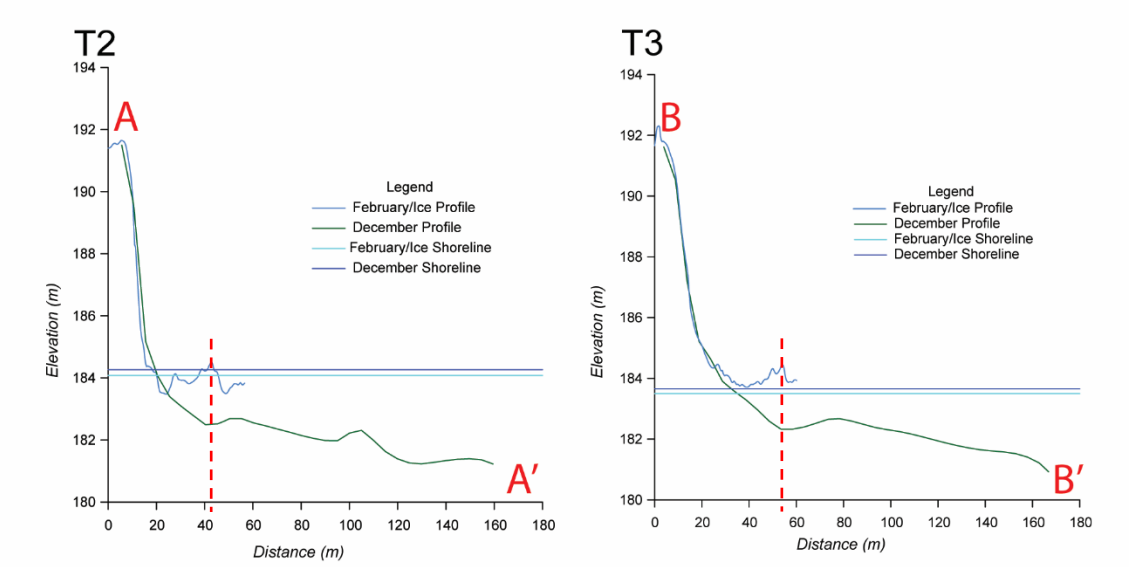

Figure 5: Profiles of ice morphology and December, March, and September bathymetry on the nearshore derived from two transects A-A' and B-B' run perpendicular to the shoreface. Red dashed lines overlay the profiles noting the relationship between the ice morphology and the December bathymetry profile.

Morphological changes

From August to November 2020, both the beach and bluff topography as well as the nearshore bathymetry changed by smoothing the profile and redistributing sediment making net volumetric change erosive (Figures 6 and 7). The net volumetric change between the August and November survey date morphology was -1.074 $m^3/m/myr$ (Table 4). The largest volume change throughout the entire study was documented during this time. The August 2020 topobathymetric map (Figure 6) indicated that a bar was present on the west end of the study area while the November shoreface showed a transformation to a smooth, uniform shoreface with a slightly offshore deposition of sediment (Figure 7). Sand appears to have been transferred into the nearshore and deposited on a transverse bar. This and the surrounding morphological change resulted in erosion that is concentrated on the shoreface and the nearshore and slight accretion in the northeast portion of the study area (Figure 7). The November storm redistributed sediment through longshore transport of sediment flowing from west to east (Figure 7).

Table 4: Summary table of case study morphological results. Description of time series given with rank of influence throughout the study period.

Timeseries	Volumetric Change (m3/m/myr)	Classification of change	Description
August 2020-November 2020	-1.074	Erosion	**Highest Rank:** a storm redistributed sediment and eroded shoreface
November 2020-December 2020	-0.338	Erosion	Third Rank: recovery from storm was net erosive
December 2020-March 2021	-0.060	Erosion	**Lowest Rank:** ice was present which lowered the overall profile
March 2021-September 2021	-0.677	Erosion	Second Rank: erosion persisted through recovery months

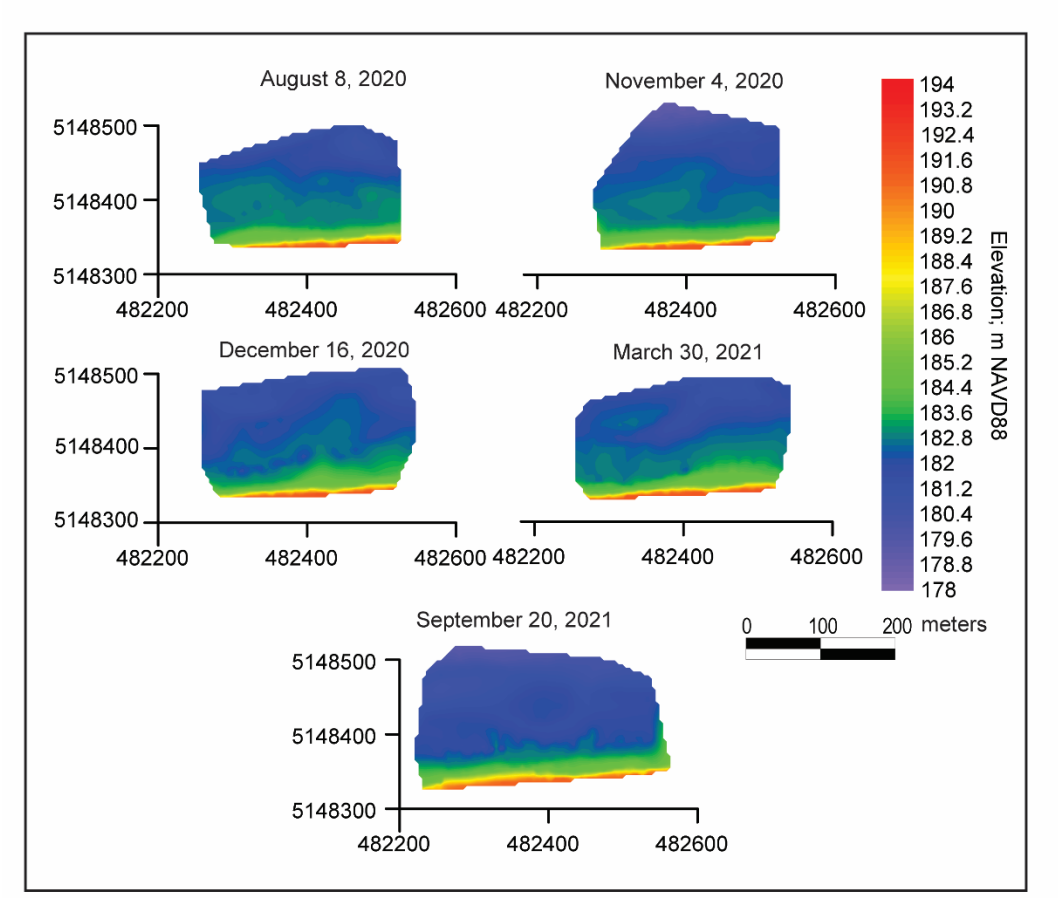

Figure 6: Topobathymetric maps from all surveys conducted. August, November, and December of 2020 and, March, and September of 2021 surveys are displayed with elevation range of 194-178 meters.

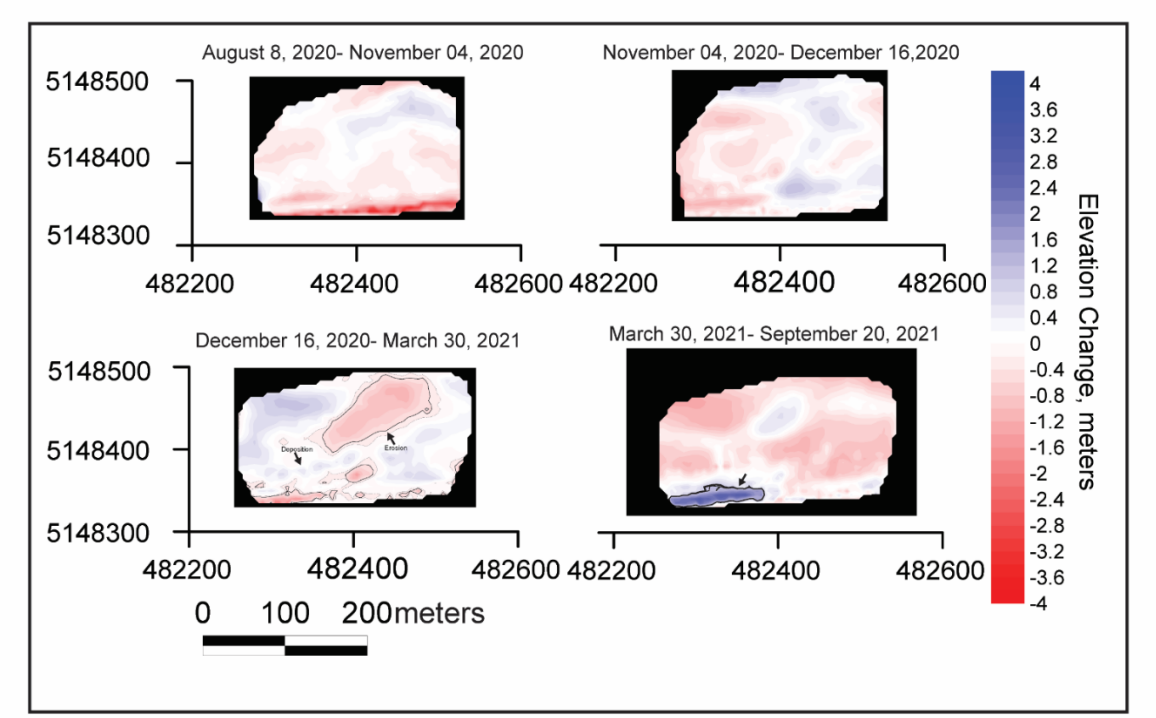

Figure 7: DEMs of Difference (DOD) between each of the surveys. August 8, 2020- November 04, 2020, November 04, 2020- December 16, 2020, December 16, 2020- March 30, 2021, March 30, 2021- September 20, 2021 are the time series combinations.

Between the November and December surveys, recovery did not occur from the November storm (Table 4, Figure 7). During the month-long period, the shoreface was redistributed with sediment with a similar evolution of the welded shoreline sandbar from the August survey (Figure 6). However, this sand bar was located slightly east of where it was in August (Figure 6). A pronounced trough developed about 30 m from the shoreline, which separated the sand bar from the foreshore (Figure 7). The net volumetric change between the November and December survey date morphology was -0.338 m^3/m/myr of erosion (Table 4). This was the third highest rank of volumetric change during the study period. During this time period, slight accretion was documented predominately on the east side of the study site with localized erosion in the southwest end of the nearshore corresponding to an area along the bluff that experienced erosion failure during that month (Figure 7).

No morphology data were collected from the December 2020 survey to ice onset, and since significant wave height data indicated calm conditions, we consider the December 2020 topobathy map to document the pre-ice morphology. The total volumetric change was -0.060 $m^3/m/myr$ (Table 4), but the localized areas of higher magnitudes of change are spatially relevant to the overall change. Significant geomorphic changes in December 2020 to March 2021 can be seen in two distinct areas in the study location (Figure 7). In the December 2020 to March 2021 subtraction map (Figure 7) where the lakeward most extent of the ice corresponds to an area of localized erosion offshore, area B with one example of z-value = -1.16 meters, and is 145 meters in length, and area A which corresponds spatially to an area of deposition. This depositional area spans 116 meters in length. Comparisons between the March profiles and the December profiles show that the previous troughs associated with the spatial position of the ice ridges had filled with sediment by the March survey date. Profile 2 A-A' (Figure 5) shows smoothing along the profile until approximately 50 meters offshore where there is approximately a half a meter of accumulation of sediment. Profile 3 B-B' (Figure 5) shows the March profile to be the inverse of the December profile starting 30 meters offshore.

During the time between March 2021 and September, 2021 there was a stark contrast between the accretion in the southwestern corner of the study site to the surrounding erosion (Figure 7). The erosion during this time covers the majority of the nearshore during the entire study period. The blue represents accretion from an approximately 50 meter long revetment that was installed after repeated bluff failure occurred (Figure 7). The net volumetric change for this time series is -0.691 meters of erosion (Table 4). The study site shows a small area of accretion in the northeast portion that corresponds to the same area of localized erosion from December 2020 to March 2021 (Figure 7). This shows partial refilling of that area but the majority of the

area and immediately surrounding the area either continuously eroded or had negligible change (Figure 7).

In comparison to the March profiles, the September profiles are lower in elevation overall (Figure 8). Profile 2 A-A' (Figure 8) shows the September profile diverting from the March profile at approximately 20 meters from the beginning of the transect only to meet again at ≈120 meters and then immediately diverge again. Profile 3 B-B' (Figure 8) has a September profile that separates from the March at ≈5 meters from the beginning of the transect. The profiles then cross at ≈115-130 meters along the transect (Figure 8). Between the two elevation profiles, September had the lowest, deepest, profile which dipped to approximately 182.5 m (Figure 8).

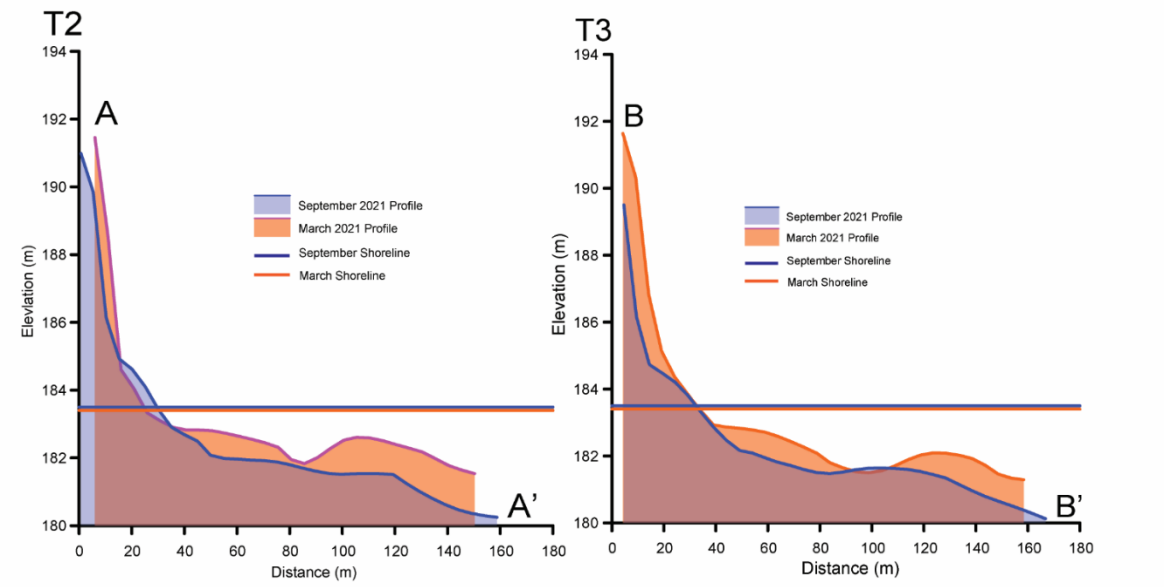

Figure 8: Elevation profiles from the March 30, 2021 and September 20, 2021 surveys accompanied by corresponding water levels to represent the shoreline position on those dates.

Discussion

Ice morphology and nearshore bathymetry

The nearshore bathymetry mapped in the December 2020 survey is considered the template for nearshore ice complex formation as it is the closest survey in time to ice onset. No storm events were documented in the wave height data between the December 2020 survey and ice onset in January 2021, thus substantial bathymetric chance between this time period is unlikely. Overlaying the December lakebed morphology with the ice morphology indicates that the initial ridge in the NIC corresponds spatially to a nearshore bar and trough located about 30 meters offshore (Figure 5, A-A'). This relationship between the ice morphology and lakebed bathymetry supports previous research that indicates NIC ridges are associated with nearshore sandbars (e.g., O'Hara and Ayers, 1972; Seibel et al., 1976); however, our data suggests that this maybe be more nuanced than previously identified, meaning more detailed and complex. In our data, the ridge crest appears to be located just above to the nearshore trough, while the bar is located just nearshore of the ridge crest (Figure 5). This is logical given that wave breaking occurs over the sandbar, leading to ice and sediment thrust onto the NIC, forming a ridge just landward of the bar.

The ice extent lines (Figure 4) from February 21 and March 13, 2021, represent where in the study area the nearshore ice complex was positioned on-average through the 2021 ice season. Multiple ice extent lines were digitized for this study that overlaid the February 21 and March 13, 2021, ice lines to a degree of variability, and two dates were chosen to show that the average ice extent carried from February to March 2021 (Figure 4). The change in the most lakeward ice extent lines of March 7 and 8, 2021 shows the dynamic behavior of the NIC, while still there is a stable nature to the ice complex (Figure 4). This stability presented itself in the average ice

extent, while the dynamic nature is illustrated in the farthest ice extent fluctuation. The dynamic nature of the shore ice extent is due in large part to hydrodynamic activity, specifically wave action. The peak wave action between the December to February time series was 2.198 meters and for the February to March time series is 2.273 meters (Table 1). After NIC generation, wave heights from during the ice season were those that interacted mostly with the farthest ice extent and contributed to the NIC deterioration.

The ice extent lines from March 7 and 8, 2021 satellite (Figure 4) show the farthest extent of NIC growth during the ice season and also the high degree of variability in the ice extent. The wave action that interacted with the farthest extent allowed for most of the wave energy to be dissipated after eroding the NIC.

The ice extent lines from February 21st and March 13th, 2021 (i.e., the average ice extent for the March 2021 ice season) represent the predominant position of the most lakeward ice ridge within the NIC (figure 4). These ice extent lines are, on the eastern side of the study site, the boundary between the localized offshore erosion and the deposition landward (Figure 9). This boundary in the ice extent acts as a seawall, effectively inhibiting wave energy from transmitting past the outer ridge. Past studies suggested that ice ridges deflect wave energy down to the lakebed resulting in sediment scour and transport (Bajorunas and Duane, 1967; Kempema, 1998). Our data indicates a similar pattern of nearshore scour just lakeward of the ice ridge (Figures 7 and 9). On the western end of the study area, along the average ice extent lines, a zone of sediment deposition is apparent between December 2020 and March 2021 (Figures 7 and 9). This area was mapped as a trough in December 2020, which was then filled in by the March 2021 survey, likely in response to in-place melting of the NIC given the spatial correlation between the average ice extent lines and the depositional zone (Figure 7, 9).

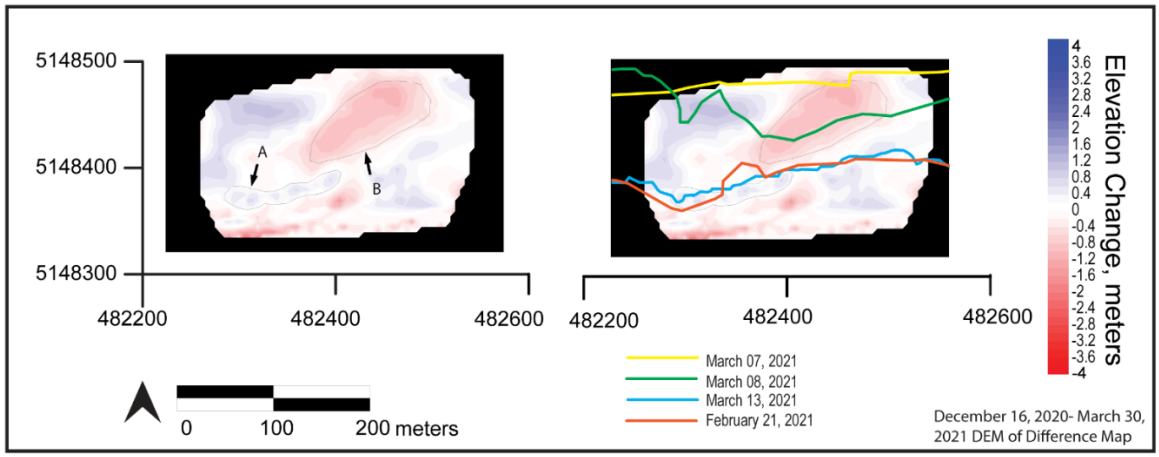

Figure 9: December 16, 2021 DEM of difference. A) Bar of accretion, B) Area of erosion, example z = -1.16 meters. December 16, 2021 DEM of difference accompanied by digitized lines of lakeward ice extent from Planet satellite imagery.

Morphological changes

Substantial variability in the magnitude and pattern of geomorphic change was documented at the study site throughout the monitoring period (August 2020 through September 2021). These changes were induced by a combination of storm events, shore ice-associated processes, and fair-weather coastal processes such as longshore transport of sand. The study site is oriented east-west, thus is exposed to large waves during storms from all northerly directions given the fetch along Lake Superior. These storm events erode sediment from the beach and upper shoreface and transport it offshore where calm wave conditions can redistribute the material across the shoreface. Similarly, storm waves can contribute to nearshore erosion lakeward of the NIC as well as facilitate NIC breakup and associated sediment transport. Along cold-climate coastlines these physical and hydrodynamic drivers of coastal change combine throughout a given year to shape the nearshore morphology though the relative importance of shore ice compared to other drivers had not been explored prior to this study.

From August 2020 to November 2020, the primary facilitator of net volumetric change was the high energy storm event that occurred on November 1, 2020 and had a peak significant wave height to 4.069 meters (Figure 3). This event resulted in substantial beach, bluff, and upper shoreface erosion and some deposition of material lakeward of the surf zone (Figure 7, Table 4). The approximately month-long period from the November 2020 survey to the December 2020 period was characterized by moderate wave conditions with a couple of low magnitude wave events as peak wave height during this period was 2.453 m (Figure 3). While morphologic recovery, defined as a return to pre-storm morphology and volume, is typically observed following a wave event (Morton, Paine, and Gibeaut, 1994), minimal recovery was documented at the site after the November storm (-0.338 m3/m/yr) (Table 4). Additional erosion was observed on the western side and some zones of accretion were observed on the eastern side, which appeared to be related to a bar welding to the shoreline (Figure 7). This pattern may be the result of longshore transport moving sand through the site. Given that wave conditions were generally calm between the December 2020 survey and ice onset in January 2021, the December 2020 topobathymetic map is used as the pre-ice morphology survey to document the geomorphic impacts associated with ice formation and breakup.

From December 2020 through March 2021, ice was present for late January through mid-March. This likely contributed to the minimal beach and upper shoreface erosion that was observed during this period (Figures 7 and 9). Overall, volumetric change was lowest during this period as compared to the other periods (Table 4), which aligns with previous research (Bamasoud and Byrne), though spatial variability in the pattern of erosion and deposition was evident throughout the site. As noted in the previous section, substantial erosion was documented just outboard of the average NIC lakeward extent and a zone of deposition was observed in

alignment with the position of the outer ridge of the NIC (Figures 7 and 9). These spatial patterns of geomorphic change affirm previous work, which documented lakebed scour in front of the NIC (Bajorunas and Duane, 1967) and deposition associated with melting of the NIC (Barnes, 1990, 1994). This zone of scour outboard of the NIC is important as it serves to both deepen the lakebed and facilitates offshore sediment transport, potentially lakeward of the depth of closure (Figures 5, 7, and 9). Deepening of the lakebed can result in waves not breaking until closer to the shore, which can enhance beach and upper shoreface erosion that as we soon documented, persisted throughout the year.

During the time between March 2021 and September 2021, the site experienced overall erosion as evidenced by a net volumetric change of -0.691 m3/m/yr (Table 4). Most of the nearshore eroded including the upper shoreface area along the western side of the site where deposition had occurred associated with the ice ridge. There was some slight accretion in the nearshore scour zone though this does not appear to completely restore all the material lost from the ice front scour (Figure 7). The localized zone of accretion documented along the beach and bluff on the western side of the site is associated with a shore protection project. During the summer of 2021 a rock revetment was constructed on the bluff to mitigate erosion and protect the Michigan Department of Transportation Roadside Park at the top of the bluff. The erosion documented throughout the site from March 2021 to September 2021 is surprising given the generally calm wave conditions observed during this period. It appears that the erosion is primarily located along the upper shoreface (i.e., the surf zone landward to the beach), which may be the result of the lakebed deepening lakeward of the NIC and an associated landward shift in where wave energy was expended (Figure 7). Future surveys are needed to document whether

there is a return to the longshore transport dominated coastal processes that were documented at the site during the fall of 2020 or if the ice has semi-permanently altered nearshore processes.

Things to be considered during the comparison of this study to previous literature would be the basin depth and ice thickness, fetch, and degree of NIC development. Additionally, more surveys will be conducted throughout the following year to document further morphological change. If water level continues to fall, erosion may persist through time and the shoreface may struggle to recover. And when faced with the prospect of shore ice presence, coastal managers should suspect to see evidence of depositional and erosional spatial distribution associated with the location of ice morphology.

Conceptual Model

The hydrodynamic influences that develop summer shores grows into fall storm activity that creates the topobathymetric profile for NIC genesis (Figure 10). Those same hydrodynamics act upon the NIC, breaking it apart while spatially changing the bathymetry of the lakebed, especially on the lakeward edge of the NIC. This new bathymetry then develops through hydrodynamics back into a somewhat summer shoreline state. However erosional impacts from the timeseries where the NIC was present persisted spatially and temporally as there was minimal accretive recovery up to September 2021. The geomorphic behavior during this study suggests that there exists a feedback system within the study area with the hydrodynamics of the environment being the dominant influence that is present in all timeseries that is represented through our proposed conceptual model. Hydrodynamics change bathymetry as energy entering the system increases, the NIC then develops, altering the topography and bathymetry during growth and break-up through hydrodynamic processes (Figure 10). These topographic and bathymetric changes persist throughout the year (Figure 10).

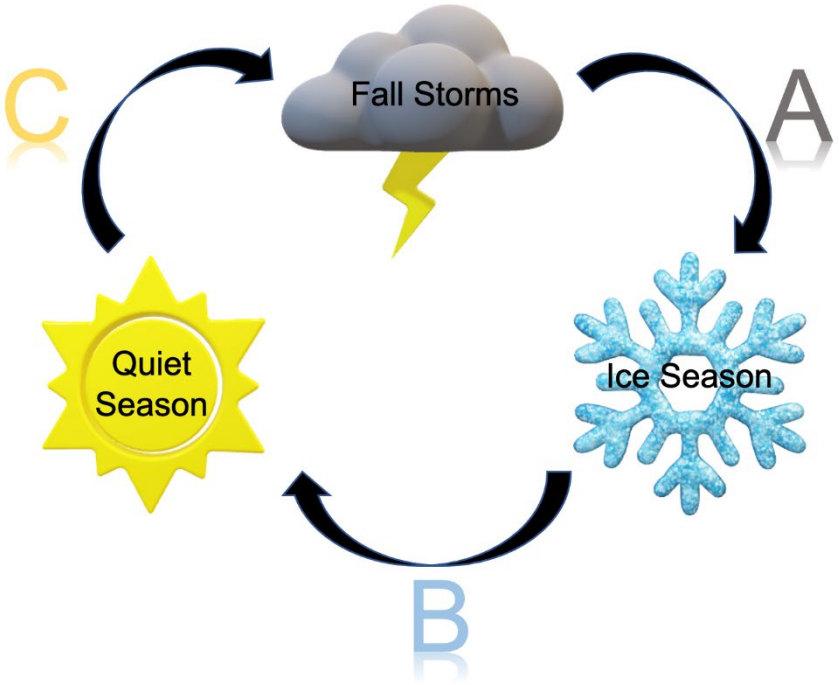

Figure 10: Conceptual model of case study results. Showing the profile change encompasses the trifecta of morphological events; Fall Storms, Ice Generation, and Ice Recession, that are all based on the same fundamental driving force; hydrodynamic activity, specifically wave action.

Conclusions

The idea of shore ice protecting or eroding (Barnes, Kempema, and Reimnitz and McCormick, 1994) the shoreline with its presence or break-up is black and white on a grey spectrum, implying the relationship of shore ice to the topography and bathymetry is more nuanced than currently thought. The effects are more spatially variable and persistent temporally. The erosive or protective effects of shore ice depend in part on pre-existing bathymetry and persist throughout the year non-linearly throughout the site. Additionally, the hydrodynamic activity present at the site were the main driving force behind the morphological change, whether it be from storm events or generating and breaking up the nearshore ice complex. As the environment evolved through the year, erosion persisted and the shoreface changed into a more linear shape. The methodology of this work promotes the novelty of our findings such that this style of high in accuracy and detail in mapping has not been applied to this subject research as of yet. Ongoing data collection shows potential for prolonged monitoring of the system and analysis of long-term shoreface recovery amidst persistent hydrodynamic activity. Continuous data collection also provides local coastal managers with a more comprehensive idea of what spatial distribution of depositional and erosional patterns are possible relative to the ice morphology present.

REFERENCES

REFERENCES

Bajorunas, L., Duane, D.B., 1967. Shifting offshore bars and harbor shoaling. J. Geophys. Res. 72, 6195–6205. https://doi.org/10.1029/JZ072i024p06195

BaMasoud, A., Byrne, M.-L., 2012. The impact of low ice cover on shoreline recession: A case study from Western Point Pelee, Canada. Geomorphology 173–174, 141–148. https://doi.org/10.1016/j.geomorph.2012.06.004

Barnes, P. W., 1990. Coastal sedimentary processes in southern Lake Michigan; their influence on coastal erosion, 1989 progress reports and accomplishments. *Open-File Report*. https://doi.org/10.3133/ofr90295

Barnes, P.W., Kempema, E.W., Reimnitz, E., McCormick, M., Weber, W.S., Hayden, E.C., n.d. Beach Profile Modification and Sediment Transport by Ice: An Overlooked Process on Lake Michigan 22.

Barnes, P.W., Kempema, E.W., Reimnitz, E., McCormick, M., 1994. The Influence of Ice on Southern Lake Michigan Coastal Erosion. Journal of Great Lakes Research 20, 179–195. https://doi.org/10.1016/S0380-1330(94)71139-4

Barnorff-Nielsen, O. E., and C. Christiansen. "Erosion, Deposition and Size Distributions of Sand." *Proceedings of the Royal Society of London. Series A, Mathematical and Physical Sciences*, vol. 417, no. 1853, 1988, pp. 335–52, http://www.jstor.org/stable/2398020. Accessed 7 Apr. 2022.

Baumann, Hannes, and Owen Doherty. "Decadal Changes in the World's Coastal Latitudinal Temperature Gradients." *PLoS ONE*, vol. 8, no. 6, 2013, doi:10.1371/journal.pone.0067596.

Bryan, M.L., Marcus, M.G., 1972. Physical Characteristics of Near-Shore Ice Ridges. ARCTIC 25, 182–192. https://doi.org/10.14430/arctic2960

EPA., "Climate Impacts on Coastal Areas." Environmental Protection Agency, 6 Oct. 2016, 19january2017snapshot.epa.gov/climate-impacts/climate-impacts-coastal-areas.html.

Dionne, J.-C., 2021. Sediment Load of Shore Ice and Ice Rafting Potential, Upper St. Lawrence Estuary, Québec, Canada. Journal of Coastal Research 9, 20.

Dionne, Jean-Claude, and Camille Laverdière. "Ice Formed Beach Features from Lake St. Jean, Quebec." *Canadian Journal of Earth Sciences*, vol. 9, no. 8, 1972, pp. 979–990., doi:10.1139/e72-082.

Douglas, Thomas A., et al. "Sources and Sinks of Carbon in Boreal Ecosystems of Interior Alaska: A Review." *Elementa: Science of the Anthropocene*, vol. 2, 2014, doi:10.12952/journal.elementa.000032.

Evenson, E. B., and Cogn, B. P. 1979. The ice-foot complex: its morphology, formation and role in sediment transport and shoreline protection. Zeitschrift fir Geomorphologie, Neue Folge, 23: 58-75.

Forbes, D.L., Taylor, R.B., 1994. Ice in the shore zone and the geomorphology of cold coasts. Progress in Physical Geography: Earth and Environment 18, 59–89. https://doi.org/10.1177/030913339401800104

Gilbert, R., 1990. A distinction between ice-pushed and ice-lifted landforms on lacustrine and marine coasts. Earth Surf. Process. Landforms 15, 15–24. https://doi.org/10.1002/esp.3290150103

Héquette, A., Desrosiers, M., Barnes, P.W., 1995. Sea ice scouring on the inner shelf of the southeastern Canadian Beaufort Sea. Marine Geology 128, 201–219. https://doi.org/10.1016/0025-3227(95)00095-G

Hubertz, Jon M. *User's guide to the wave information studies (WIS) wave model, version 2.0*. Vol. 27. US Army Engineer Waterways Experiment Station, 1992.

Kalke, H., McFarlane, V., Schneck, C., Loewen, M., 2017. The transport of sediments by released anchor ice. Cold Regions Science and Technology 143, 70–80. https://doi.org/10.1016/j.coldregions.2017.09.003

Kempema, E.W., Holman, R.A., 1994. Video Monitoring of Nearshore Ice in Southern Lake Michigan. Journal of Great Lakes Research 20, 196–205. https://doi.org/10.1016/S0380-1330(94)71140-0

Kempema, E.W., Reimnitz, E., Barnes, P.W., n.d.1998. ANCHOR-ICE FORMATION AND ICE RAFTING IN SOUTHWESTERN LAKE MICHIGAN, U.S.A. 9.

Kilibarda, Z., Shillinglaw, C., 2015. A 70year history of coastal dune migration and beach erosion along the southern shore of Lake Michigan. Aeolian Research 17, 263–273. https://doi.org/10.1016/j.aeolia.2014.09.002

Lantuit, Hugues, et al. “The Arctic Coastal Dynamics Database: A New Classification Scheme and Statistics on Arctic Permafrost Coastlines.” *Estuaries and Coasts*, vol. 35, no. 2, 2011, pp. 383–400., doi:10.1007/s12237-010-9362-6.

Miner, J.J., Powell, R.D., 1991. An Evaluation of Ice-Rafted Erosion Caused by an Icefoot Complex, Southwestern Lake Michigan, U.S.A. Arctic and Alpine Research 23, 320. https://doi.org/10.2307/1551610

Morton, Robert A., et al. “Stages and Durations of Post-Storm Beach Recovery, Southeastern Texas Coast, U.S.A.” *Journal of Coastal Research*, vol. 10, no. 4, 1994, pp. 884–908, http://www.jstor.org/stable/4298283. Accessed 7 Apr. 2022.

Nordhaus, William D. “Geography and Macroeconomics: New Data and New Findings.” *Proceedings of the National Academy of Sciences*, vol. 103, no. 10, 2006, pp. 3510–3517., doi:10.1073/pnas.0509842103.

O’Hara, N. W., and J. C. Ayers. 1972 Stages of shore ice development. In *Proc. 15th Conf. On Great Lakes Res.,* International Association for Great Lakes Research 521-535.

Philipp, Marius, et al. “Trends in Satellite Earth Observation for Permafrost Related Analyses—a Review.” *Remote Sensing*, vol. 13, no. 6, 2021, p. 1217., doi:10.3390/rs13061217.

Reimnitz, E., Hayden, E., McCormick, M., Barnes, P.W., 1991. Preliminary Observations on Coastal Sediment Loss through Ice Rafting in Lake Michigan. Journal of Coastal Research 7, 653–664.

Roland, C.J., Zoet, L.K., Rawling, J.E., Cardiff, M., 2021. Seasonality in cold coast bluff erosion processes. Geomorphology 374, 107520. https://doi.org/10.1016/j.geomorph.2020.107520

Seibel, E., Carlson, C.T., Maresca, J.W., 1976. Ice Ridge Formation: Probable Control by Nearshore Bars. Journal of Great Lakes Research 2, 384–392. https://doi.org/10.1016/S0380-1330(76)72301-3

Theuerkauf, Ethan J, et al. “Patterns and Processes of Beach and Foredune Geomorphic Change along a Great Lakes Shoreline: Insights from a Year-Long Drone Mapping Study along Lake Michigan.” *Shore & Beach*, 2021, pp. 46–55., doi:10.34237/1008926.

Wang, J., Bai, X., Hu, H., Clites, A., Colton, M., Lofgren, B., 2012. Temporal and Spatial Variability of Great Lakes Ice Cover, 1973–2010*. Journal of Climate 25, 1318–1329. https://doi.org/10.1175/2011JCLI4066.1

Wang, J., Kessler, J., Hang, F., Hu, H., Clites, A.H., Chu, P., n.d. Great Lakes Ice Climatology Update of Winters 2012-2017: Seasonal Cycle, Interannual Variability, Decadal Variability, and Trend for the period 1973-2017 14.